JOURNAL OF THERMOPHYSICS AND HEAT TRANSFER
Vol. 20, No. 1, January–March 2006

Turbine Rotor with Various Tip Configurations Flow and Heat Transfer Prediction

Huitao Yang,* Hamn-Ching Chen,† and Je-Chin Han‡
Texas A&M University, College Station, Texas 77843-3123

A numerical study is performed to simulate the leakage flow and heat transfer on a flat tip, a double squealer tip, and a single suction-side squealer tip of a scaled up General Electric-E^3 blade. The simulations for a nonrotating blade at a pressure ratio of 1.2 are in reasonable agreement with the experimental data on the blade tip and suction side, but the heat transfer coefficients were overpredicted on the pressure side. Numerical simulations were then performed for nonrotating and rotating blades under high-temperature, high-pressure ratio, and high Mach number conditions to investigate the blade tip leakage flow and heat transfer characteristics under more realistic engine operating conditions. The simulation results show that the heat transfer coefficient decreases with increasing squealer cavity depth, but the shallow squealer cavity is the most effective configuration to reduce the overall heat load. The blade rotation produces a dramatic increase of heat transfer coefficient on the shroud. The tip leakage flow pattern and local heat transfer coefficient distributions on the blade tip are also significantly changed due to the rotation-induced centrifugal and Coriolis forces. However, the area-averaged heat transfer coefficient on the blade tip is only slightly affected by the blade rotation.

Nomenclature

A	=	heat transfer area, m^2
C	=	tip gap clearance, % of blade span
D	=	depth of squealer cavity, % of blade span
h	=	local convective heat transfer coefficient, $q/(T_w - T_{\text{in},0})$, W/m$^2 \cdot$ K
P	=	local static pressure, Pa
Q	=	total heat flux, W
q	=	heat flux, W/m^2
St	=	Stanton number, $h/(\rho_{\text{in}} v_{\text{in, relative}} C_p)$
T	=	temperature, K
y^+	=	dimensionless distance of the first grid to the wall
ρ	=	density, kg/m^3

Subscripts

in	=	inlet of the cascade
out	=	outlet of the cascade
t	=	stagnation flow condition or total value
w	=	wall

I. Introduction

TURBINE blade tips are subjected to high thermal load and represent one of the most susceptible areas for blade cracking and failure. The tip is directly exposed to the leakage flow driven by the pressure difference between the blade pressure and suction sides. Because of the high velocity, thin boundary layer, and high temperature associated with the leakage flow, the blade tip experiences high heat load, and it is one of the most difficult regions to be cooled effectively. To reduce the tip leakage flow and heat transfer, different tip configurations are investigated. One of the commonly used configurations is a squealer tip, which acts as a labyrinth seal and increases the flow resistance. This leads to low leakage flow rate and low heat transfer rate in the blade tip region.

Many numerical studies have been conducted recently to investigate the blade tip heat transfer. Ameri et al.[1] used the TRAF3D.MB code to study the effect of squealer tip on rotor blade heat transfer. Ameri et al.[2] studied the effects of tip gap clearance and casing recess on heat transfer and stage efficiency for several squealer blade tip geometries. Ameri and Bunker[3] performed a computational study to investigate the detailed heat transfer distributions on blade tip surfaces for a large power generation turbine and compared their result with the experimental data of Bunker et al.[4] Ameri[5] computed the flow and heat transfer of a blade tip with a mean-camberline strip tip. Yang et al.[6,7] numerically studied the flow and heat transfer around the General Electric-E^3 (GE-E^3) blade with a flat tip and a squealer tip. The predicted heat transfer coefficients are in reasonable agreement with the experimental results of Azad et al.[8,9]

Experimental studies have also been conducted to investigate the heat transfer and flow on the gas turbine blade tip. Azad et al.[8,9] studied the flow and heat transfer on the first-stage blade tip of an aircraft engine turbine (GE-E^3) by liquid crystal technique. The results show that the squealer tip can reduce the heat transfer coefficient compared with the flat tip configuration. Azad et al.[10] also studied the effect of the squealer geometry arrangement on gas turbine blade tip heat transfer. Papa et al.[11] measured average and local mass transfer coefficients on a squealer tip and winglet-squealer tip using the naphthalene sublimation technique. They also presented the flow visualization of the tip surface using an oil dot technique. Kwak et al.[12] and Kwak and Han[13,14] measured heat transfer coefficients on the tip and near-tip regions of both plane and squealer tip blades by transient liquid crystal technique. They showed that the heat transfer coefficient is higher on the tip than that of the near-tip region. Also, the heat transfer coefficient on the cavity floor will be reduced with increasing squealer rim. The single suction-side squealer is the best configuration to reduce the heat transfer coefficient on the cavity floor. Jin and Goldstein[15] measured local mass transfer on a simulated high-pressure turbine blade and near-tip surfaces. Dey and Camci[16] investigated the effect of tip desensitization, through the use of winglets, on the flow characteristic for an axial turbine blade. Their results show that the pressure-side winglet will reduce the tip leakage flow considerably. Because of the limitations in experimental facilities, most of the experimental studies were performed under relatively low inlet/outlet pressure ratio and nonrotating conditions, which are far from real engine operating conditions. It is, therefore,

Received 7 December 2004; presented as Paper 2005-573 at the AIAA 43rd Aerospace Sciences Meeting and Exhibit, Reno, NV, 10–13 January 2005; revision received 8 March 2005; accepted for publication 9 March 2005.

*Research Assistant, Turbine Heat Transfer Laboratory, Department of Mechanical Engineering. Student Member AIAA.

†Professor, Ocean Engineering Program, Department of Civil Engineering. Senior Member AIAA.

‡M.C. Easterling Chair Professor, Turbine Heat Transfer Laboratory, Department of Mechanical Engineering. Associate Fellow AIAA.

desirable to investigate the effects of high-pressure ratio and high rotating speed on blade tip heat transfer characteristics under more realistic engine conditions.

The present study focuses on the numerical prediction of flow and heat transfer of GE-E^3 blade with different blade tip configurations including a flat tip, a double-squealer tip, and a single suction-side squealer tip as tested by Kwak and Han.[13] The numerical results for the non-rotating, low temperature and low pressure ratio cases were compared with the experimental data of Kwak and Han.[13] Calculations were also performed for both the nonrotating and rotating blades at high total temperature, high Mach number, and high-pressure ratio conditions to provide a detailed understanding of the blade tip leakage flow and heat transfer characteristics under more realistic engine conditions.

II. Computational Details

Computations were performed for the blade tip flow and heat transfer around a GE-E^3 blade using the commercial software package FLUENT. This code solves compressible Reynolds averaged Navier–Stokes equations using the finite volume method to discretize the equations. GAMBIT grid-generation software was used to generate unstructured grids, with grid clustering in the near-wall and tip regions.

To facilitate a direct comparison with the experimental data of Kawk and Han,[13] the present calculations were performed for a three-times scaled-up model of the GE-E^3 blade. Figure 1 shows the geometry and numerical grids for the GE-E^3 blade with various blade tip configurations. Note that the blade geometry used by Kwak and Han[13] and the present study is a two-dimensional blade with the same blade profile in the spanwise direction from the blade root to tip. Furthermore, the present two-dimensional blade profile and the inlet flow angle are identical to those at the tip section of the actual GE-E^3 blade because the Kwak and Han[13] study and the present study are concerned with the heat transfer characteristics in the blade tip region. Figure 1a shows the three tip configurations, including the flat tip, double-squealer tip, and single suction-side squealer tip. Figure 1b is the schematic of the double-squealer blade tip geometry with selected cross-sectional planes that will be used later to show the flow structures around the blade tip region. Detailed grid distribution is shown in Fig. 1c. The scaled-up blade has a constant axial chord length of 8.61 cm and an aspect ratio (span to the chord) of 1.4. The blade leading-edge pitch is 9.15 cm. The depths of the squealer cavity are 0.254, 0.508, and 0.762 cm, which are 2.1, 4.2, and 6.3% of the blade span, respectively. In the present simulations, the blade tip clearance is kept constant with a tip gap of 1.97 mm or 1.5% of the blade span. The effect of different tip gap clearances on the blade tip heat transfer has been investigated experimentally by Azad et al.[8,9] and numerically by Yang et al.[6,7] and will not be repeated here.

The computational domain consists of a single blade with periodic conditions imposed along the boundaries in the circumferential (pitch) direction. The inlet boundary is placed at one-half chord length upstream of the blade so that simple uniform inflow boundary conditions can be employed. Calculations were performed first for the nonrotating case using the experimental conditions of Kwak and Han.[13] The total temperature, 300 K, and total pressure, 130.0 kPa, are specified along with the inlet flow angle, 32 deg, and turbulence intensity level, 9.7%. The corresponding Mach number at the inlet is 0.25. The exit boundary is located at one chord length downstream of the blade trailing edge to provide appropriate resolution of the tip leakage flow and passage vortices. The static pressure is specified as 108.3 kPa at the exit. Therefore, the inlet total pressure to the outlet static pressure ratio ($P_{\text{in},t}/P_{\text{out}}$) is 1.2. On the blade surface, the no-slip condition and uniform wall temperature conditions were specified.

For completeness, simulations were also performed for the same three-times scaled-up GE-E^3 blade using typical operating conditions for a real turbine with a blade tip radius of 35.56 cm (14 in.) under both nonrotating and rotating conditions. This enables us to evaluate the effects of rotation, high temperature, high Mach number, and high inlet/outlet pressure ratio on the overall heat transfer in the blade tip region. A rotating speed of 9600 rpm is used in the present rotating blade simulation. The inlet total temperature is specified at 1479 K (2662°R) and the blade surface temperature is 1035 K. The inlet turbulence intensity is 9.7%, and the inlet flow angle is 32 deg. The total pressure at the inlet is 1.675 MPa, and the static pressure at the exit is 1.027 MPa. This gives a inlet/outlet pressure ratio, $P_{\text{in},t}/P_{\text{out}}$, of 1.63, which is significantly higher than the 1.20 used in the experiments of Kwak and Han.[13] For convenience, the simulations at high total temperature and high inlet/outlet pressure ratio cases are denoted as high parameter, whereas the low inlet/outlet pressure ratio and low total temperature cases corresponding to the experimental conditions are denoted as low parameter in the following discussions. For the rotating cases, the blade domain is rotating with a relative inlet flow angle equal to 32 deg, whereas the shroud remains stationary. All other conditions are kept the same as the high-parameter stationary case to facilitate a detailed understanding of the effects of blade rotation under realistic turbine working conditions.

For blade tip leakage flow and heat transfer simulations, Yang et al.[6,7] showed that the Reynolds stress model (RSM) of Hanjalic[17] performs slightly better than the high Reynolds number k–ε model (Launder and Spalding[18]) and RNG k–ε model (Hanjalic[17]). In all cases, nonequilibrium wall function is employed to handle the near-wall turbulence. The y^+ value is adjusted iteratively to about 30 by splitting or merging the near-wall grids to satisfy the requirement of nonequilibrium wall function. For heat transfer calculations, an isotropic eddy viscosity model with constant turbulent Prandtl number is employed to represent the turbulent heat flux in the energy equation. Unless otherwise indicated, the results presented in this paper are based on the RSM model, the tip clearance is 1.5% of the blade span, and the depth of the squealer cavity is 4.2% of the blade

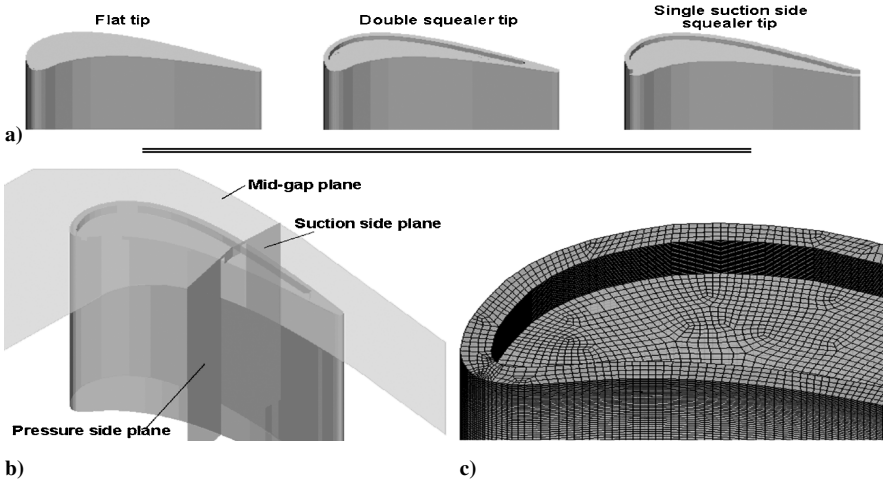

Fig. 1 Blade geometry and numerical grid: a) three tip configurations, b) grid schematic with different cross section planes, and c) typical grid of squealer blade tip.

span. A total of 13 simulations were performed for the nonrotating and rotating blades with various blade tip configurations as shown in Table 1.

All of the cases presented are converged to residual levels of the order of 10^{-5} and to less than 0.01% error in the mass flow rate between the inlet and exit of the computational domain. Typically, 800 iterations are required for convergence. For the squealer tip configuration considered here, typically the calculation is performed with about 1 million nodes, with the grid point distribution outside the squealer tip region being similar to that in the flat tip study. The grid independency has been studied by Yang et al.[6]

III. Results and Discussion

A. Pressure and Velocity

Figure 2 shows a comparison of the pressure ratio ($P_{\text{in},t}/P$) distributions for both the nonrotating and rotating cases with three blade

Table 1 Summary of simulated cases

		Double squealer			Single suction side squealer		
Working conditions	Flat tip	2.1%	4.2%	6.3%	2.1%	4.2%	6.3%
Nonrotating, low parameters	×	×	×	×	×	×	×
Nonrotating, high parameters	×		×			×	
Rotating, high parameters	×		×			×	

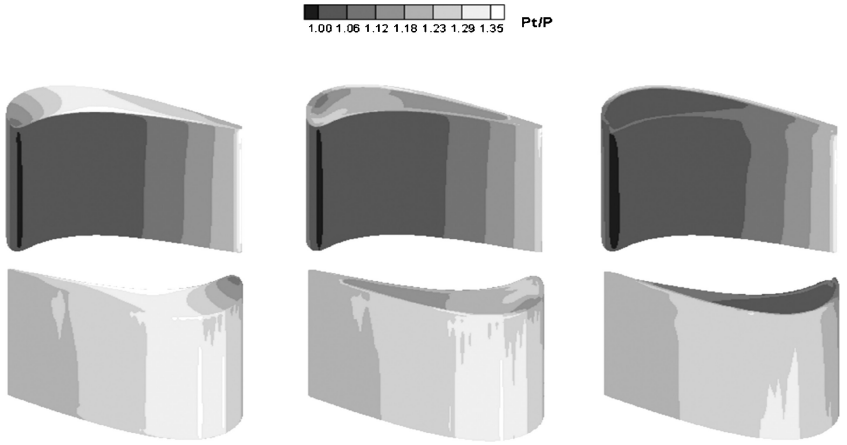

a) Low parameters, nonrotating

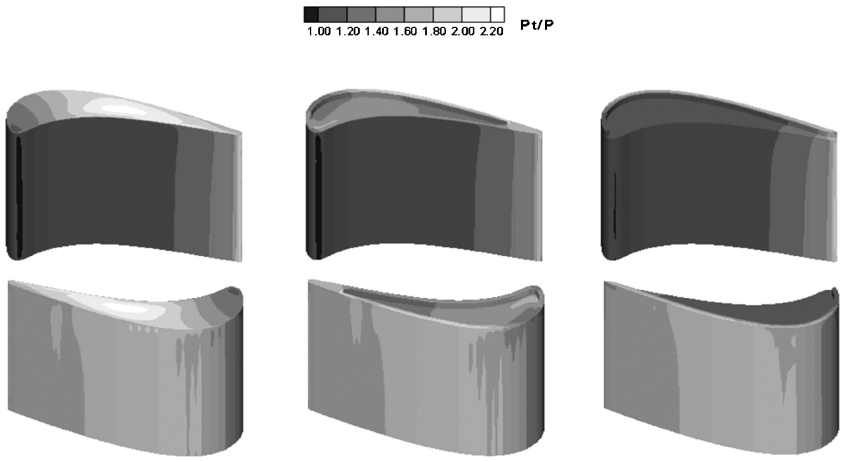

b) High parameters, nonrotating

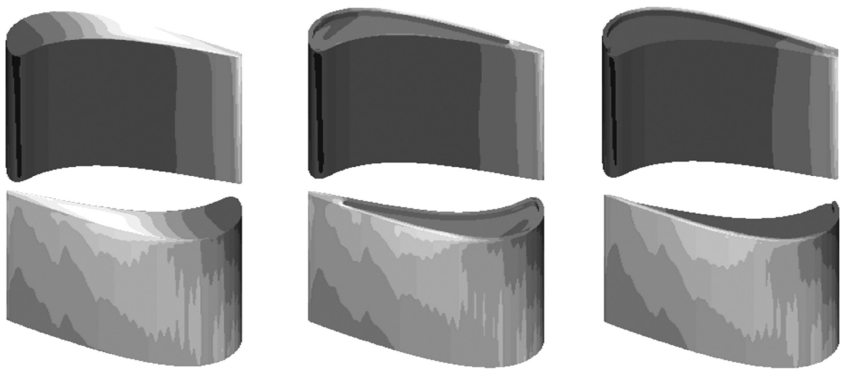

c) High parameters, rotating

Fig. 2 Pressure ratio $P_{\text{in},t}/P$ distributions comparison on pressure and suction sides of various flow conditions; left to right: flat tip, doubler-squealer tip, and single-suction-side squealer tip.

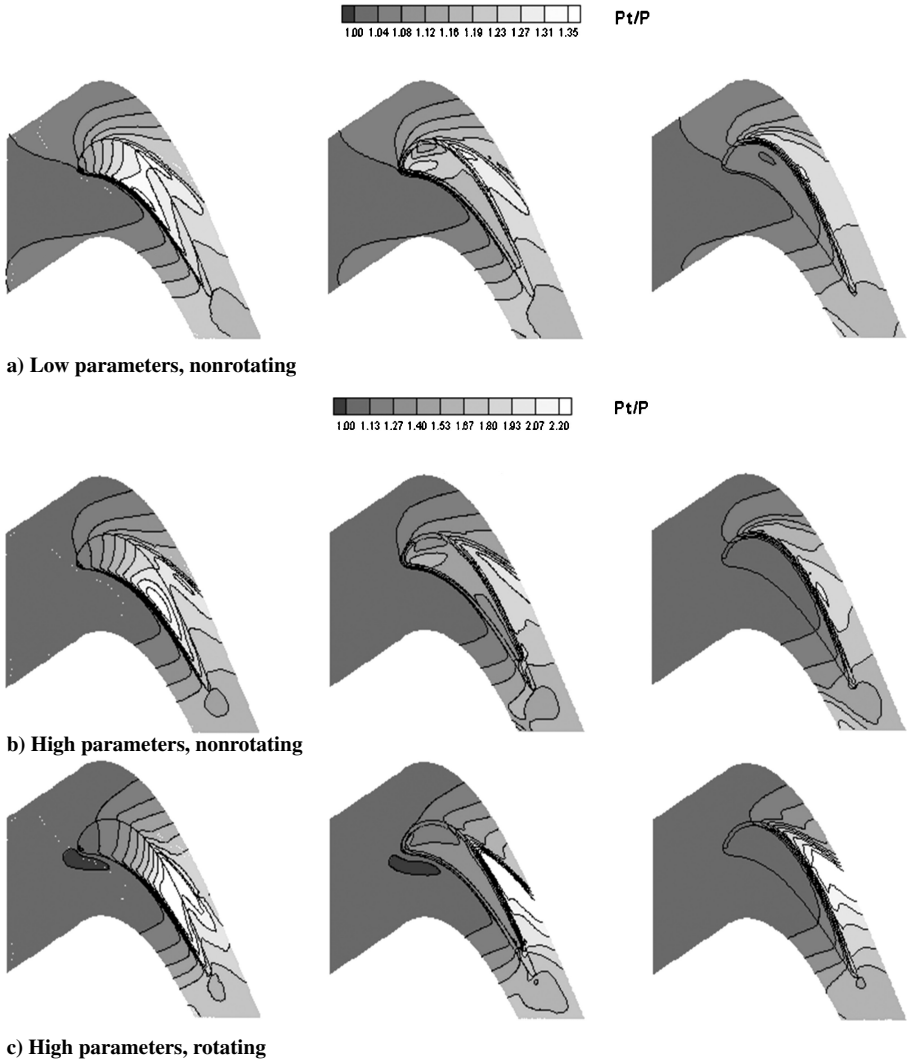

Fig. 3 Pressure ratio $P_{\text{in},t}/P$ distributions comparison on shroud of various flow conditions; left to right: flat tip, double-squealer tip, and single suction-side squealer tip.

tip configurations: flat tip, double-squealer tip, and single suction-side squealer tip. For completeness, the corresponding pressure ratio ($P_{\text{in},t}/P$) distributions on the shroud of all three tip configurations are also shown in Fig. 3 to facilitate a more detailed understanding of the flow in the blade tip region. In both Figs. 2 and 3, generally the high value of $P_{\text{in},t}/P$ ratio corresponds to low static pressure and high velocity. The pressure pattern on the shroud matches the corresponding pressure ratios on the blade tip because the pressure variation across the narrow tip gap clearance is relatively small. It is seen that the pressure ratio is quite low on the pressure side, but becomes significantly higher on the suction side. Because of the favorable pressure gradient between the pressure and suction sides of the blade, the flow is accelerated through the gap between the blade tip and the shroud. For the nonrotating cases, note that the effect of tip leakage flow is confined to a small region near the blade tip, and the pressure ratio on the other portions of the blade side shows a two-dimensional distribution. Under the rotating conditions, however, the pressure contours becomes highly three dimensional on the blade suction side due to the migration of blade passage vortex toward the blade tip region as a result of the rotation-induced centrifugal and Coriolis forces. On the blade pressure side, the pressure ratio is only slightly affected by the blade rotation. On the other hand, the high pressure ratio, that is, high-velocity, region on the blade suction side was pushed downstream toward the trailing edge and also radially outward to the blade tip region. Moreover, the overall pressure ratio increases significantly on both the blade suction side and tip region in comparison with the stationary case. It is quite clear that the centrifugal and Coriolis forces tend to increase the blade tip leakage flow and produce stronger leakage vortices on the suction side of the blade tip region for both the flat tip and squealer tip configurations.

For the nonrotating flat tip configuration, under experimental conditions, that is, low $T_{\text{in},t}$ and $P_{\text{in},t}/P_{\text{out}}$, high-pressure ratios were observed in the midchord region and along the edge of the pressure-side blade tip, indicating the presence of strong leakage flow through the midchord section of the blade tip gap clearance. For the double-squealer tip configuration, the pressure ratio is high on the squealer rim due to local flow acceleration in the narrow gap on the top of the squealer rim, but drops significantly inside the squealer cavity due to flow separation behind the pressure-side squealer rim. The pressure ratio inside the squealer cavity is much lower than that observed in the flat tip case, indicating that the tip leakage flow is significantly reduced in the double-squealer tip configuration. For the single suction-side squealer tip configuration, a high-pressure-ratio region is again observed on top of the squealer rim. However, the low-pressure-ratio region on the pressure side was extended over most of the blade tip surface with a drastic reduction of the tip leakage flow across the suction side squealer rim. Based on the pressure ratio distributions on the blade tip and shroud, it is quite clear that the single suction-side squealer tip is the most effective configuration for the reduction of the tip leakage flow among the three different blade tip configurations considered in the present study.

For the nonrotating cases with high inlet/outlet pressure ratio and high total temperature, that is, high parameters, conditions, the

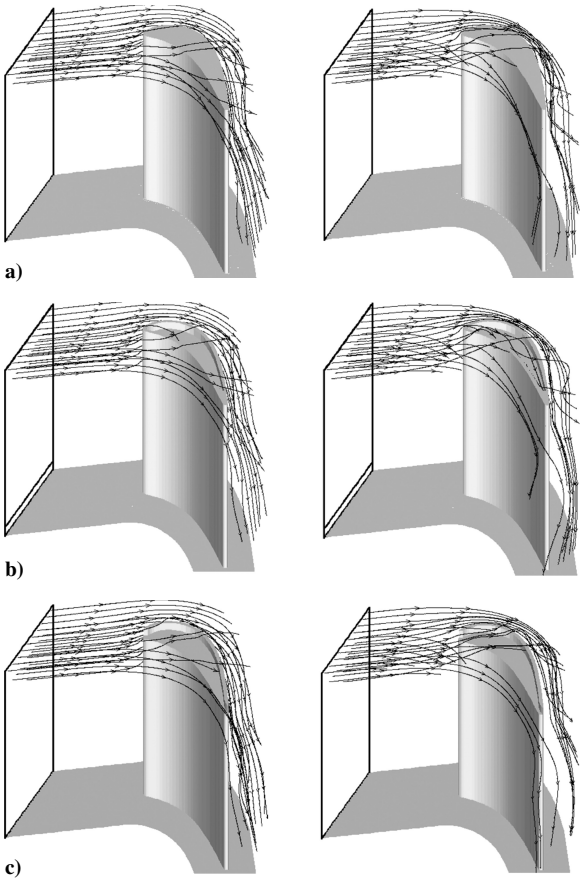

Fig. 4 Pathlines comparison for a) flat tip, b) double-squealer tip, and c) single suction-side squealer tip configurations, as well as high parameter nonrotating (left) and rotating cases (right).

overall pressure ratio level is significantly higher than the corresponding low parameter cases. Furthermore, the high-pressure ratio regions on the suction side and the blade tip were shifted downstream for both the flat and squealer tip configurations as seen in Figs. 2 and 3. Consequently, the strongest tip leakage flow was observed in the downstream section of the blade, where the blade thickness is relatively small. For the rotating case, the blade tip velocity is 357.5 m/s (9600 rpm), nearly twice of the blade inlet velocity of 183 m/s, but the inlet/outlet pressure ratio, total temperature, and the relative inlet flow angle are kept the same as the nonrotating high parameter case. Note from Fig. 2 that the blade rotation results in a significant increase of pressure ratio in the blade tip gap region and on the blade suction side. In general, the rotation tends to increase the leakage flow and produce a large leakage vortex on the suction side for both the flat and squealer tip configurations. Furthermore, the leakage flow was observed to shift toward the trailing edge, where the blade is relatively thin and harder to cool. Similar pressure ratio patterns were also observed on the shroud, as shown in Fig. 3. Details of the leakage vortices and their effects on the blade tip and shroud heat transfer will be discussed later.

Figure 4 shows the pathlines around three blade tip configurations under various flow conditions. For completeness, the pathlines and Mach number contours at the midgap between the blade tip and shroud are shown in Fig. 5 to facilitate a detailed understanding of the blade tip leakage flow for both the nonrotating and rotating cases. For the flat tip configuration, the fluid accelerates through the tip gap and combines with the mainstream flow on the suction side to form a tip leakage vortex. The velocity of tip leakage vortex is slower than the flow in other regions. For the double-squealer tip, the flow structure around the tip is more complicated than the other two cases. In addition to the tip leakage vortex near the blade suction side, another vortex was formed inside the squealer cavity when the fluid enters the squealer cavity from the leading edge and pressure side of the blade tip. The vortex rolls down the pressure-side squealer rim to form a large recirculation flow region inside the squealer cavity. It then rolls up across the suction-side squealer rim

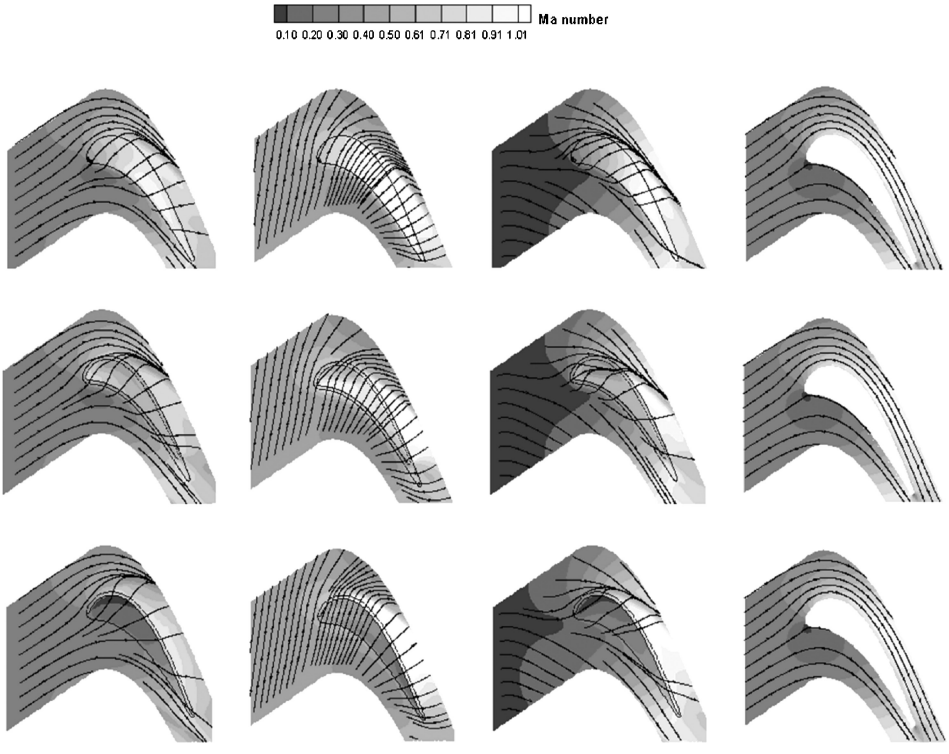

Fig. 5 Streamlines comparison and Mach number contours on midgap plane of various flow conditions; top to bottom: flat tip, doubler-squealer tip, and single suction-side squealer tip.

and merges into the suction-side tip leakage vortex. It is also found that the velocity of the vortex inside the squealer cavity decreases from the leading edge to the trailing edge. For the single suction-side squealer tip configuration, a leakage vortex was formed along the junction of the blade tip and the squealer rim. The vortex rolls up across the squealer rim and merges into the tip leakage vortex on the blade suction side. Note that the structure of the tip leakage flow for the nonrotating cases does not change significantly between the low parameter and high parameter conditions.

For the rotating cases, the pathlines are plotted using the relative velocity in a rotating reference frame. For detailed understanding of the flow pattern in the blade tip region, two different sets of pathlines were released at the cascade inlet. The first set of pathlines was released at the same location as the nonrotating cases, whereas a second layer of pathlines was released inside the shroud boundary layer. In general, the tip leakage flow in the blade tip gap region is still driven by the pressure gradient between the pressure and suction sides of the blade, similar to that observed for the nonrotating cases. However, the tip leakage flow pattern is significantly modified by the rotation-induced centrifugal and Coriolis forces. Furthermore, the pathlines near the stationary shroud wall are deflected toward the pressure side of the blade because the flow inside the shroud boundary layer lags behind the rotating blade due to the viscous effects.

Figure 5 shows a comparison of the pathlines and Mach number contours for both the nonrotating and rotating high parameter cases to provide a more detailed understanding of the effects of rotation on the tip leakage flow patterns. For the nonrotating cases shown in Fig. 5a, the tip leakage flow at the midgap plane is driven from the pressure side to the suction side, and the pathlines converge to form a leakage vortex in the suction-side blade passage. When the blade is rotating at the designed speed of 9600 rpm, the absolute flow velocity and the approach angle are adjusted so that the inflow angle relative to the rotating blade remains the same at 32 deg. Figures 5b and 5c show the pathlines and Mach number contours at the midgap plane for the rotating cases in the Earth-fixed, that is, absolute velocity, and rotating, that is, relative velocity, reference frames, respectively. The pathlines and Mach number contours at midspan plane are shown in Fig. 5d to illustrate the three-dimensional flow pattern under rotating conditions. Note that the pathlines at the midspan plane for the rotating cases have the same relative inlet flow angle as that observed for the nonrotating cases because the flow in the midspan is not directly affected by the blade tip leakage flow. In the midgap plane, however, the flow at the turbine inlet was deflected toward the pressure side (Fig. 5c) because the approach flow inside the shroud boundary layer lags behind the rotating blade due to the viscous shear stress exerted by the stationary shroud. In the midgap between the blade tip and the shroud, the leakage flow is subjected to the combined effect of shroud viscous force and the pressure gradients between the pressure and suction sides of the rotating blade. It is quite clear that the pressure gradient across the tip gap is strong enough to overcome the viscous resistance of the stationary shroud and push the tip leakage flow from the pressure side to suction side. Note that the absolute velocity of the tip leakage flow must be faster than the rotating blade to push the fluid from the pressure side to the suction side of the rotating blade. In general, the flow pathlines over the blade tip are quite similar between the nonrotating and rotating cases, indicating that the tip leakage flow is still dominated by the pressure gradients across the tip gap under the rotating conditions.

Figure 6 shows a comparison of the streamlines and Mach number contours at two streamwise cross sections, that is, the pressure-side

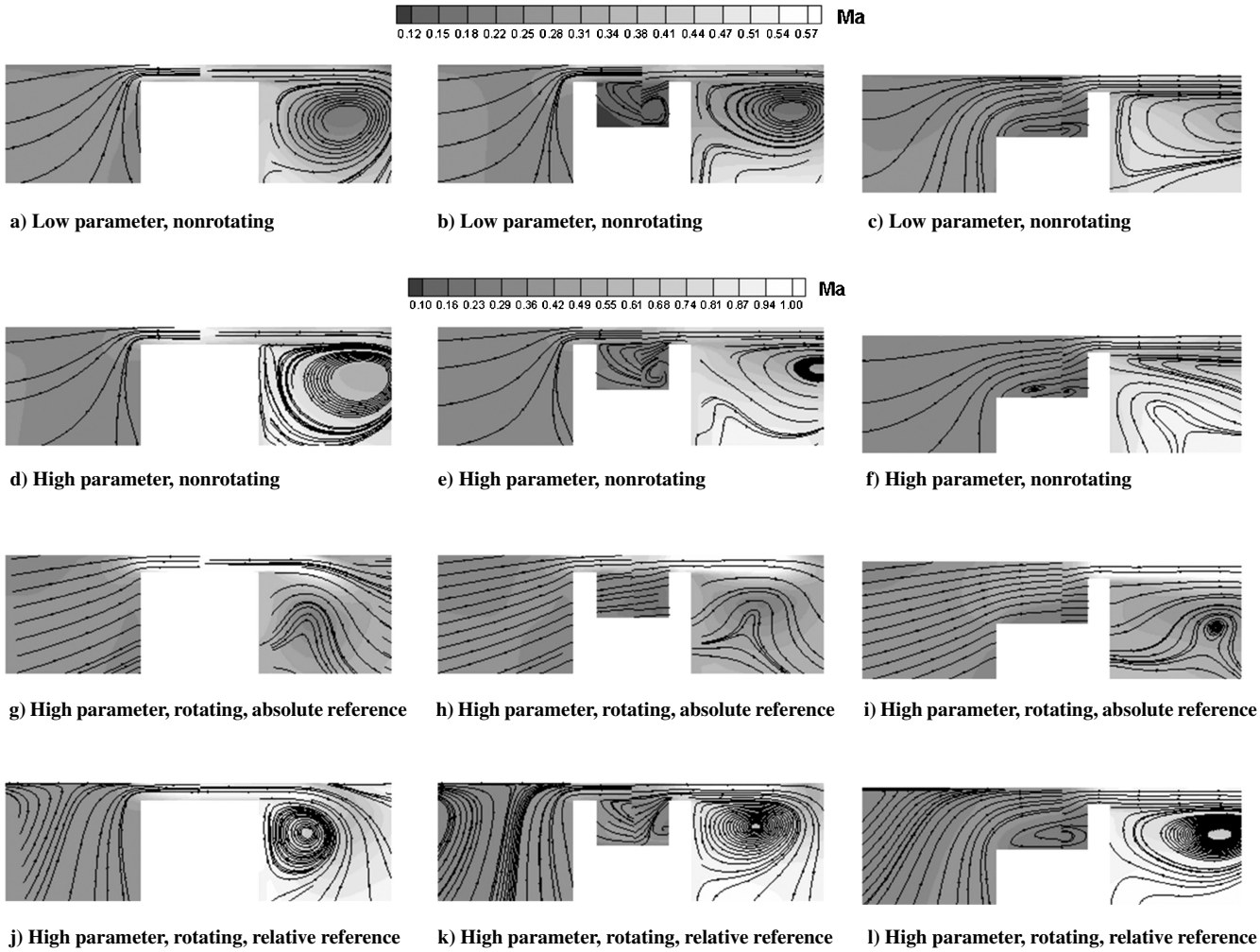

Fig. 6 Streamlines comparison and Mach number contours at pressure- and suction-side cross sections for nonrotating and rotating cases: left to right: flat tip, double-squealer tip, and single suction-side squealer tip.

and suction-side planes in Fig. 1 for the flat tip, double-squealer tip, and single suction-side squealer tip for both the nonrotating and rotating cases with 4.2% tip clearance. To understand in detail the secondary flow patterns induced by the pressure gradient and blade rotation for different blade tip configurations, the pressure-side and suction-side planes were chosen to be perpendicular to the blade pressure and suction sides, respectively, and intersect at the camber line. For all three different blade tip configurations, low velocity exists on the pressure side, whereas the velocity on the suction side is significantly higher. Fluid is driven by the pressure difference between the pressure and suction sides of the blade and accelerates through the blade tip region. The tip leakage flow is combined with the inlet passage flow to form the leakage vortex in the suction side, as shown in the pathlines in Fig. 4. For the double-squealer tip, a recirculation flow region was observed inside the squealer cavity due to flow separation behind the pressure-side squealer rim. For single suction-side squealer tip, a large recirculation region is observed in front of the rim.

For the nonrotating cases, the leakage flow structures for the high parameter cases are similar to those for the low parameter cases on the pressure suction and in the squealer cavities, although the Mach number is significantly higher for the high parameter cases. As noted earlier (Fig. 3), the tip leakage flow increases for the high parameter cases and the location of the maximum tip leakage was pushed toward the trailing edge. Consequently, the location and shape of the leakage vortex changed significantly at the selection suction-side plane for both the double- and single suction-side squealer tip configurations.

For the rotating cases, the absolute velocity of the leakage flow is very high near the stationary shroud as seen from the Earth-fixed reference frame. However, it is not possible to see the recirculation region inside the squealer cavity in Earth-fixed frame because the fluid moves together with the blade at a very high absolute velocity. For completeness, the pathlines and Mach number contours are also plotted in a blade-fixed reference frame using relative velocities as shown in Figs. 6j–6l for a better understanding of the tip leakage flow under rotating conditions. Note that the blade rotation has significantly changed the size and shape of the leakage vortices for both the flat and squealer tip configurations. Because of the rotation-induced centrifugal force, the passage flow is pushed outward in the radial direction. The effect of rotation on passage flow migration is most noticeable on the pressure side of shroud boundary layer because the passage flow in that region has relatively low momentum and can, therefore, be easily deflected by the centrifugal force. When the radially outward passage flow impinges on the stationary shroud surface, a portion of the flow is pushed from the pressure side through the blade tip gap toward the suction side. The remaining passage flow is pushed away from the rotating blade because it has a slower absolute velocity due to the viscous effects inside the shroud boundary layer. On the suction side, the blade rotation also induced radially outward flow, which tends to reduce the size of the tip leakage vortex and push it closer to the suction side rim. However, the rotation effect is less obvious because the suction-side passage flow possesses significantly higher momentum and the centrifugal force is not strong enough to produce appreciable changes in the suction-side flow pattern.

B. Heat Transfer Distribution

Figure 7 shows a comparison of the predicted and measured heat transfer coefficients on the blade tip for a double-squealer tip

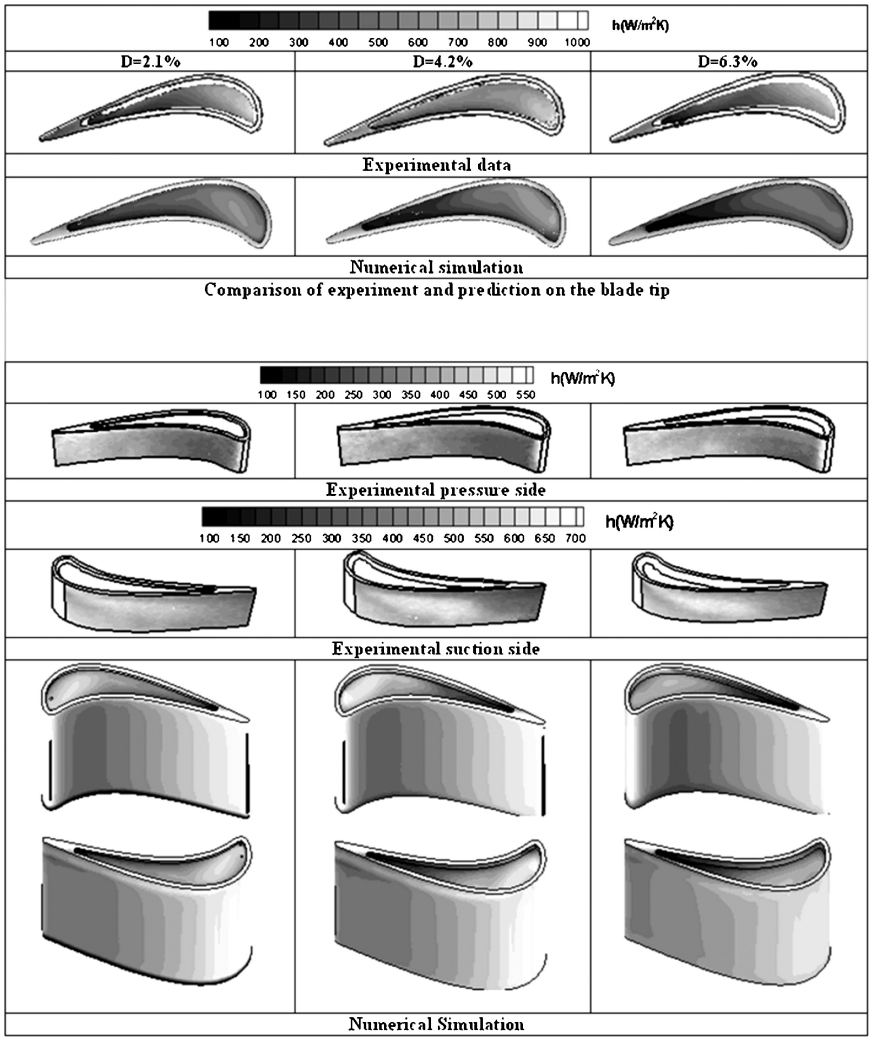

Fig. 7 Heat transfer coefficient of double-squealer tip comparison between experimental data and numerical predictions.

configuration with three different cavity recesses. For simplicity, the simulation results are presented using two sets of contour levels, which are identical to those used in the tip and suction-side measurements. Both the experiment and simulation show high heat transfer coefficients on the squealer rims due to flow acceleration on the top of the rims. On the bottom of the squealer cavity, the heat transfer coefficient is significantly lower due to the low-speed separation inside the squealer cavity. In general, the heat transfer coefficient inside the squealer cavity reduces as the cavity depth increases. This can be attributed to the increase of flow recirculation zone and the reduction of the tip leakage flow rate for deeper cavity cases as shown in Fig. 6.

On the pressure side of the near-tip region, the numerical simulations predicted similar heat transfer pattern to those observed in the experiment. However, the predicted level of heat transfer coefficients on the pressure side is about 25% higher than the corresponding measurements and shares the same level as suction side. Note that there are no experimental data around the leading edge due to the limitation on the view angle of the camera. Both the numerical and experimental results show that the heat transfer coefficient is higher near the trailing edge in comparison with that observed near the midchord region. Also, the heat transfer coefficient around the blade tip is higher than that far below the blade tip.

On the suction side of the near-tip region, the predicted heat transfer level is similar to the measured value. Both the experiments and simulations show a high heat transfer coefficient region along the suction-side blade tip. The high heat transfer coefficient in this region is clearly caused by the tip leakage vortices shown earlier in Figs. 4 and 6. However, the numerical simulations predicted somewhat smaller tip leakage vortices, which did not extend as far downward as those observed in the corresponding experiments. Also note that the heat transfer coefficients on the blade suction side are lower for the deepest cavity in comparison with other shallower cavity cases. This decrease of heat transfer coefficients with increasing cavity depth can be attributed to the reduction of tip leakage vortex strength in deeper cavities as seen in Fig. 6.

Figure 8 shows the measured and predicted heat transfer coefficients for the single suction-side squealer tip configuration. It is seen that the heat transfer coefficient is high near the pressure-side edge of the blade tip, but decreases gradually along the flow direction toward the suction-side squealer rim. The lowest heat transfer coefficient is observed in the stagnation flow region near the root of the squealer rim due to the deceleration of leakage flow along the junction of the squealer rim and blade tip surface. Both the measurements and calculations indicate that the heat transfer coefficient on the blade tip decreases as the cavity depth increases from 2.1 to 6.3%. This can clearly be attributed to the reduction of tip leakage flow with increasing cavity depth as shown earlier in Fig. 6. On the other hand, the heat transfer coefficient on the blade suction side is fairly insensitive to the change in cavity depth. In general, the numerical simulations predicted similar levels of heat transfer on the blade tip and the suction side, as was also the observation in the experimental data. However, the heat transfer coefficient on the pressure side is overpredicted.

Figure 9 shows a comparison of Stanton number St distributions on the rotor blade surface for various blade tip configurations under

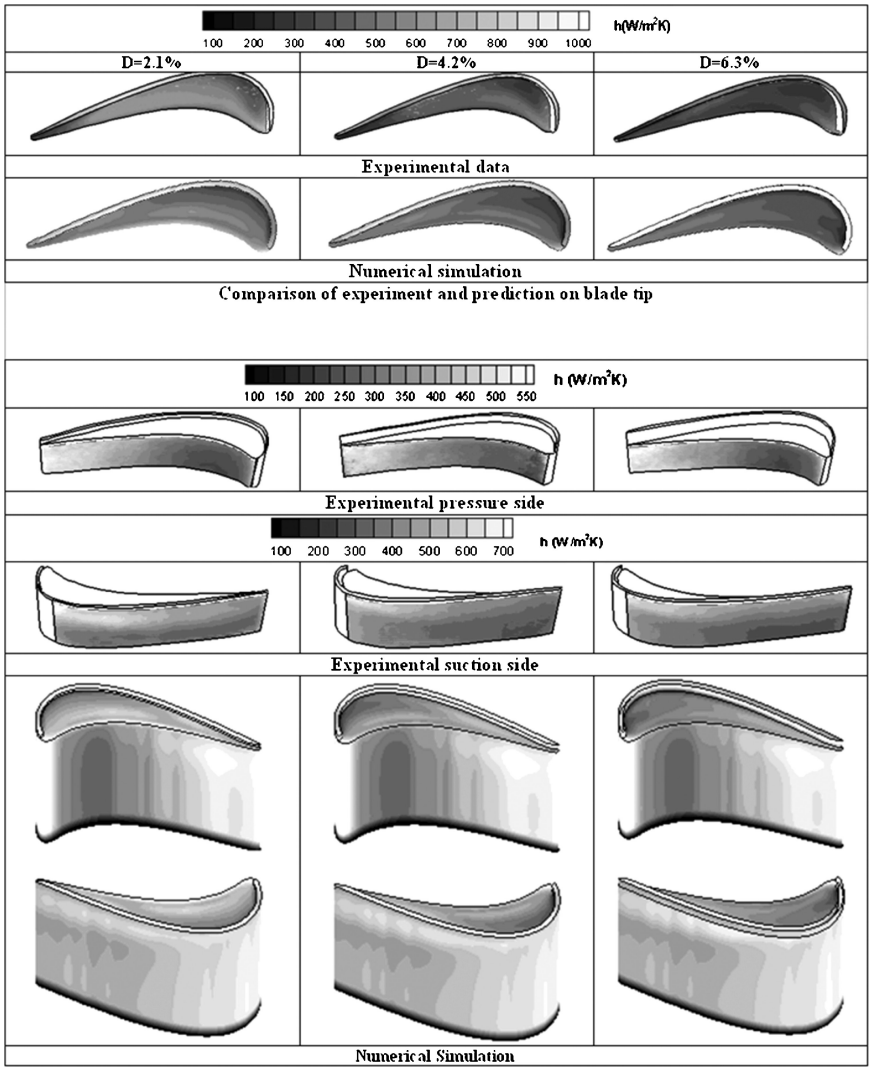

Fig. 8 Heat transfer coefficient of suction-side squealer tip comparison between experimental data and numerical predictions.

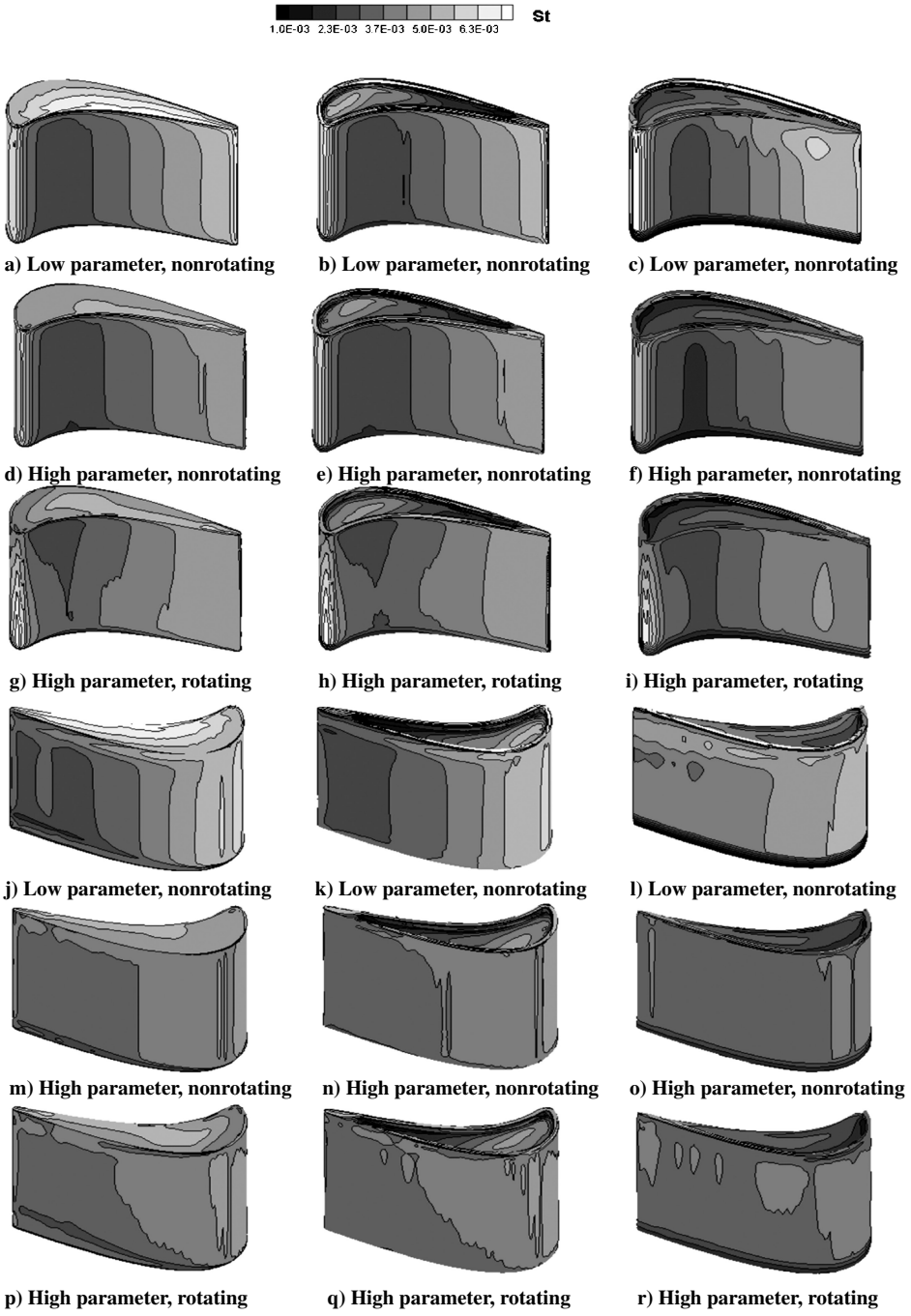

Fig. 9 Comparison of Stanton number on the blade surface: left to right: flat tip, double-squealer tip, and single suction-side squealer tip.

both nonrotating and rotating conditions. Note that the inflow velocity (183 m/s) and density (3.8 kg/m^3) for the high parameter cases are about 2.12 and 2.60 times the corresponding velocity (86.27 m/s) and density (1.46 kg/m^3) for the low parameter cases. This implies that the actual heat transfer coefficient for the high parameter case will be 5.5 times of that of the low parameter case if the Stanton number is the same for both cases. Also note that the Stanton number distributions for the low parameter cases are simply the dimensionless form of the heat transfer coefficient distributions shown earlier in Figs. 7 and 8. Therefore, we will focus on the effects of high parameter, that is, high total temperature and high-pressure ratio, and rotation in this section. For all three blade tip configurations, note that the Stanton numbers for the high parameter cases are considerably lower than those observed for the low parameter cases. However, the actual heat transfer coefficient is significantly higher for the high parameter cases because the reference heat transfer coefficient ($\rho_{\text{in}} C_p V_{\text{in}}$) for high parameter cases is about 5.5 times of that of the low parameter cases.

As noted earlier, the effect of rotation tends to increase the tip leakage flow and push the location of maximum leakage flow toward the trailing edge. However, the tip leakage flow is still dominated by the pressure gradients across the blade tip gap for all three different blade tip configurations considered. Consequently, the overall heat transfer pattern and the average level of the Stanton number for the rotating and nonrotating cases are quite similar, even though the local Stanton number distributions are affected by the blade rotation. As mentioned earlier, Ameri et al.[1] also studied the blade tip heat transfer on the rotating GE-E^3 blade with flat and double-squealer tips using slightly different boundary conditions and rotating speed. They used the exact GE-E^3 blade geometry with three-dimensional twisted blade sections, which is different from the three times scaled-up blade with two-dimensional GE-E^3 tip profile considered in the

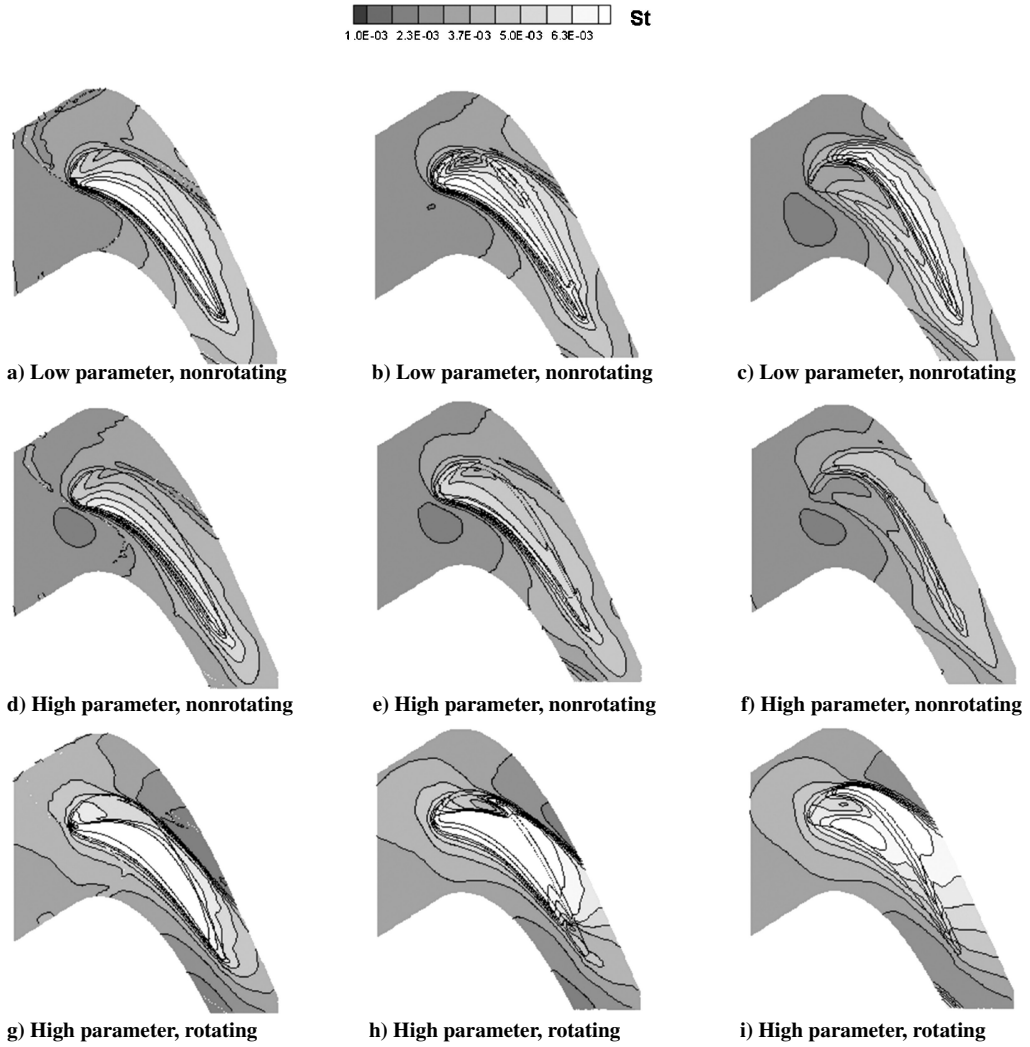

Fig. 10 Comparison of the Stanton number on the shroud: left to right: flat tip, double-squealer tip, and single suction-side squealer tip.

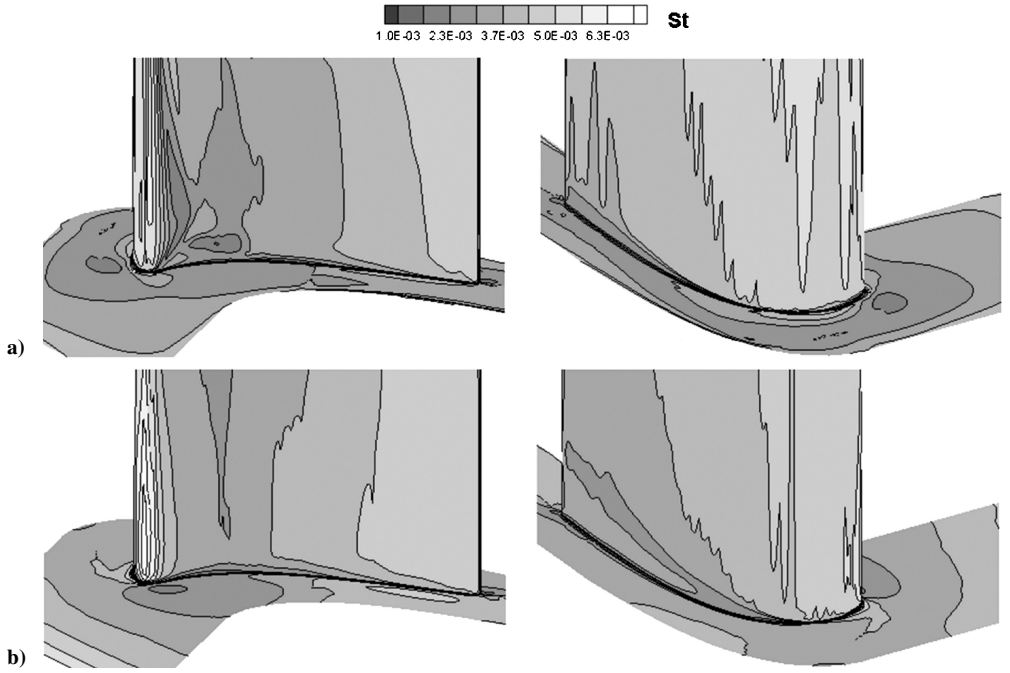

Fig. 11 Comparison of Stanton number on the hub and root of blade, high parameter, pressure side (left) and suction side (right): a) nonrotating and b) rotating.

present study. In general, the Stanton number distributions in the tip region of the present two-dimensional blade are in reasonable agreement with those obtained by Ameri et al.[1] for the exact GE-E^3 blade. Note that the present simulations predicted a higher Stanton number on the squealer rim than the cavity floor, which is consistent with the experimental data of Kwak and Han.[13] This is somewhat different from the results obtained by Ameri et al.,[1] which show a higher Stanton number on the cavity floor.

For the nonrotating cases, the Stanton numbers are nearly two dimensional except near the blade root and tip regions, where the heat transfer coefficients are affected by the horseshoe vortex and blade tip leakage vortex, respectively. Under the rotating conditions, however, the Stanton number distributions on both the pressure and suction sides of the blade become three dimensional due to the migration of blade passage vortex under the action of centrifugal and Coriolis forces. The Stanton number increases significantly at the blade leading edge and on the pressure side around the blade–hub junction. On the blade suction side, the Stanton number increases near the blade tip region, but reduces significantly along the blade–hub junction toward the trailing edge. It is quite clear that the rotation-induced centrifugal and Coriolis forces significantly changed the horseshoe vortex along the blade–hub junction as well as the blade tip leakage flow.

Figure 10 shows the Stanton number distributions on the stationary shroud surface for both the nonrotating and rotating cases. For all three different blade tip configurations, the Stanton number is found to increase dramatically under rotating conditions. The high heat transfer coefficients on the stationary shroud can be attributed to the sharp increase of velocity and temperature gradients in the shroud boundary layer. In addition to the blade tip and shroud heat transfers, note the predicted heat transfer coefficients around the blade root and hub junction for high parameter nonrotating and rotating cases, as shown in Fig. 11. Along the blade–hub junction, the flow is highly three dimensional due to the presence of horseshoe vortices in the corner region. In general, the swirling motion of the horseshoe vortex produces higher velocity and temperature gradients and increases the heat transfer coefficients along the blade–hub junction. For the rotating case, the size of the horseshoe vortex on the pressure side is significantly reduced. On the suction side, a low heat transfer strip is extended from the leading edge of the blade–hub junction toward the trailing edge as a result of the passage vortex migration under the rotating conditions.

C. Heat Load of Various Blade Tips

To evaluate the performance of various blade tip configurations for heat load reduction, it is desirable to compare the total heat flux $Q = h \times A \times \Delta T$ for each case. Under the same temperature difference (which is reasonable assumption for the large amount of tip leakage flow), the heat load rate can be defined as $h \times A$, where A is the total surface area of the blade tip region including the cavity wall, as shown in Fig. 12 marked by bold line.

Figure 13a shows the area-averaged heat transfer coefficients for various tip configurations under the low parameter conditions. It is clearly seen that the squealer tip configurations is quite effective in reducing the heat transfer coefficients. Also note that the area-averaged heat transfer coefficients decreases with increasing squealer cavity depth for both the double-squealer and single suction-side squealer tips. In general, the double-squealer tip is more effective than the single suction-side squealer tip in terms of the reduction of area-averaged heat transfer coefficients. However, the surface area of the double-squealer tip configuration is also considerably larger than the other two configurations, as seen in Fig. 12. To obtain a more meaningful comparison of the heat transfer characteristics, it is desirable to compare the total heat flux or the heat load rate for various blade tip configurations as shown in Fig. 13b. When compared to the flat tip case, the shallow cavity with 2.1% cavity depth was found to be most effective for both the double and single suction-side squealer configurations. For deeper cavity depths, the reduction in heat transfer coefficient is completely offset by the increase of the blade tip surface area with very little additional benefit in the heat load reduction.

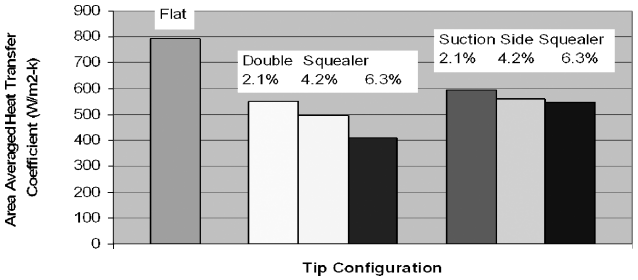

a) Low parameter, nonrotating, area average heat transfer coefficient

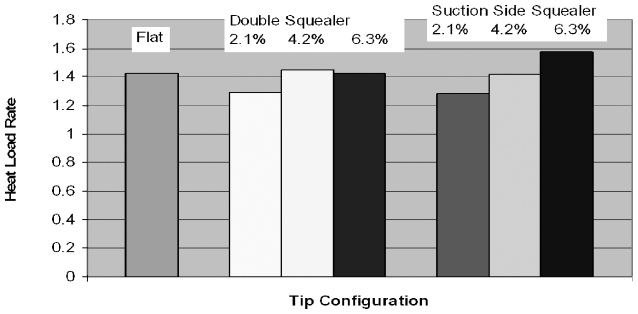

b) Low parameter, nonrotating, heat load rate

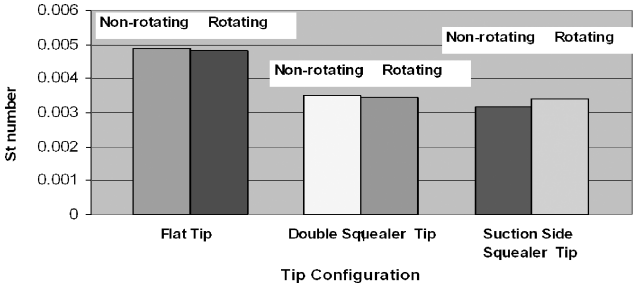

c) High parameter, area-averaged Stanton number

Fig. 13 Averaged heat transfer coefficient, heat load rate, and Stanton number comparison for various blade tip configurations.

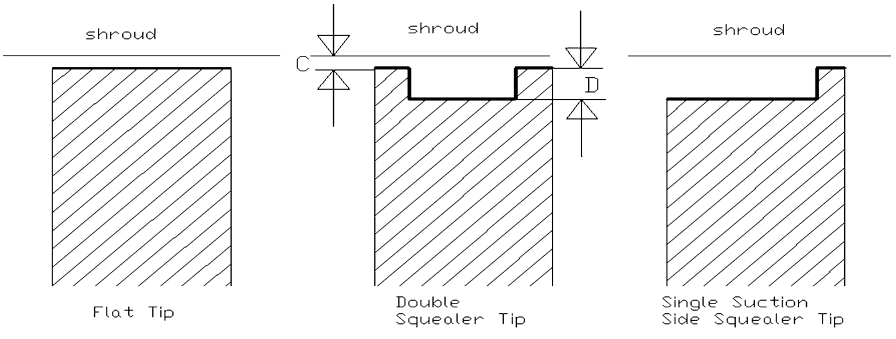

Fig. 12 Heat transfer area of various tip configurations.

For completeness, the area-averaged Stanton number for high parameter cases with 4.2% cavity depth are also shown in Fig. 13c for various blade tip configurations under nonrotating and rotating conditions. Similar to the low parameter cases, the area-averaged Stanton numbers for high parameter cases also reduce significantly for both the double and single suction-side squealer tip configurations. However, the suction-side squealer tip is more effective than the double-squealer tip configuration in reducing the area-averaged Stanton number and overall heat load rate under high parameter conditions. As noted earlier, the rotation-induced centrifugal buoyancy and Coriolis forces significantly changed the blade tip leakage flow and local heat transfer coefficient distributions. However, the area-averaged Stanton numbers shown in Fig. 13c are only slightly affected by the blade rotation for the three different blade tip configurations considered in the present study. This suggests that the primary influence of the blade rotation is to redistribute the blade tip leakage flow and local heat transfer coefficients. Because the overall heat load is relatively insensitive to the effects of the blade rotation, it is possible to obtain the area-average heat transfer coefficients for real engine conditions (with 1.5% tip clearance) based on nonrotating experiments at the same high parameter operation conditions.

IV. Conclusions

Numerical simulations of flow and heat transfer were performed for three different blade tip configurations: flat tip, double-squealer tip, and single suction-side squealer tip. The predicted heat transfer coefficients on the blade tip and suction side compared reasonably well with the experimental data, but the heat transfer coefficients in the near-tip region of pressure side were overpredicted. Both the experimental and numerical results show that the single suction-side squealer tip is the best configuration to reduce the tip leakage flow and lower the heat transfer coefficient on the squealer cavity floor on the blade tip. For both the double-squealer tip and single suction-side squealer tip, the heat transfer coefficient on the cavity floor also decreases with increasing cavity depth. However, the heat load rate was found to increase with increasing cavity depth because the available heat transfer area increases at a faster rate than the reduction in heat transfer coefficient. Therefore, it is desirable to use the tip configuration with a shallow squealer cavity to reduce the overall heat load. For the 1.5% tip clearance cases considered here, the area-averaged Stanton number and the heat load rate are only slightly affected by the blade rotation. However, the heat transfer coefficient on the stationary shroud is significantly higher under the rotating conditions due to dramatic increases of the velocity and temperature gradients in the shroud boundary layer. The heat transfer coefficients on the pressure and suction sides of the blade are also significantly changed due to the passage vortex migration induced by the blade rotation.

Acknowledgment

The project was partially supported by the U.S. National Science Foundation under Grant CTS-9903972.

References

[1]Ameri, A. A., Steinthorsson, E., and Rigby, D. L., "Effect of Squealer Tip on Rotor Heat Transfer And Efficiency," American Society of Mechanical Engineers, ASME Paper 97-GT-128, June 1997.

[2]Ameri, A. A., Steinthorsson, E., and Rigby, D. L., "Effects of Tip Clearance and Casing Recess on Heat Transfer and Stage Efficiency in Axial Turbines," *Journal of Turbomachinery*, Vol. 121, No. 4, 1999, pp. 683–693.

[3]Ameri, A. A., and Bunker, R. S., "Heat Transfer and Flow on the First Stage Blade Tip of a Power Generation Gas Turbine: Part 2: Simulation Results," *Journal of Turbomachinery*, Vol. 122, No. 2, 2000, pp. 272–277.

[4]Bunker, R. S., Baily, J. C., and Ameri, A. A., "Heat Transfer and Flow on the First Stage Blade Tip of a Power Generation Gas Turbine: Part 1: Experimental Results," *Journal of Turbomachinery*, Vol. 122, No. 2, 2000, pp. 272–277.

[5]Ameri, A. A., "Heat Transfer and Flow on the Blade Tip of a Gas Turbine Equipped With a Mean-Camberline Strip," *Journal of Turbomachinery*, Vol. 123, No. 4, 2001, pp. 704–708.

[6]Yang, H., Acharya, S., Ekkad, S. V., Prakash, C., and Bunker, R.,"Flow and Heat Transfer Predictions for a Flat-Tip Turbine Blade," American Society of Mechanical Engineers, ASME Paper GT-2002-30190, June 2002.

[7]Yang, H., Acharya, S., Ekkad, S. V., Prakash, C., and Bunker, R., "Numerical Simulation of Flow and Heat Transfer Past a Turbine Blade with a Squealer-Tip," American Society of Mechanical Engineers, ASME Paper GT-2002-30193, June 2002.

[8]Azad, G. M. S., Han, J. C., Teng, S., and Boyle, R., "Heat Transfer and Pressure Distributions on a Gas Turbine Blade Tip," *Journal of Turbomachinery*, Vol. 122, No. 4, 2000, pp. 717–724.

[9]Azad, G. M. S., Han, J. C., and Boyle, R., "Heat Transfer and Pressure Distributions on the Squealer Tip of a Gas Turbine Blade," *Journal of Turbomachinery*, Vol. 122, No. 4, 2000, pp. 725–732.

[10]Azad, G. M. S., Han, J. C., Bunker, R. S., and Lee, C. P., "Effect of Squealer Geometry Arrangement on a Gas Turbine Blade Tip Heat Transfer," *Journal of Heat Transfer*, Vol. 124, No. 3, 2002, pp. 452–459.

[11]Papa, M., Goldstein, R. J., and Gori, F., "Effects of Tip Geometry and Tip Clearance on the Mass/Heat Transfer from a Large-Scale Gas Turbine Blade," American Society of Mechanical Engineers, ASME Paper GT-2002-30192, June 2002.

[12]Kwak, J. S., Ahn, J., Han, J. C., Lee, C. P., Boyle, R., and Gaugler, R.,"Heat Transfer Coefficient on the Squealer Tip and Near Tip Region of a Gas Turbine Blade with Single Squealer," American Society of Mechanical Engineers, ASME Paper GT2003-38907, June 2003.

[13]Kwak, J. S., and Han, J. C., "Heat Transfer Coefficient on a Gas Turbine Blade Tip and Near Tip Regions," *Journal of Thermophysics and Heat Transfer*, Vol. 17, No. 3, 2003, pp. 297–303.

[14]Kwak, J. S., and Han, J. C., "Heat Transfer Coefficient on the Squealer Tip and Near Squealer Tip Regions of a Gas Turbine Blade," American Society of Mechanical Engineers International Mechanical Engineering Congress and Exposition, Paper IMECE 2002-31109, Nov. 2002.

[15]Jin, P., and Goldstein, R. J., "Local Mass/Heat Transfer on a Turbine Blade Tip," 9th International Symposium on Transport Phenomena and Dynamics of Rotating Machinery, Feb. 2002.

[16]Dey, D., and Camci, C., "Aerodynamic Tip Desensitization of An Axial Turbine Rotor Using Tip Platform Extensions," American Society of Mechanical Engineers, ASME Paper 2001-GT-0484, 2001.

[17]Hanjalic, K., "Advanced Turbulence Closure Models, A View of Current Status and Future Prospects," *International Journal of Heat and Fluid Flow*, Vol. 15, No. 3, 1994, pp. 178–200.

[18]Launder, B. E., and Spalding, D. B., "The Numerical Computation of Turbulent Flows," *Computer Models in Applied Mechanics and Engineering*, Vol. 3, No. 2, 1974, pp. 269–289.